

# Structural Consequences of Anionic Host- Cationic Guest Interactions in a Supramolecular Assembly

*Michael D. Pluth, Darren W. Johnson, Géza Szigethy, Anna V. Davis, Simon J. Teat, Allen G. Oliver,  
Robert G. Bergman, Kenneth N. Raymond\**

Contribution from the Department of Chemistry, University of California, Berkeley, CA 94720-1460  
and Chemistry Division, Lawrence Berkeley National Laboratory, Berkeley, California, 94720, USA

**RECEIVED DATE (to be automatically inserted after your manuscript is accepted if required  
according to the journal that you are submitting your paper to)**

TITLE RUNNING HEAD: Supramolecular Structural Analysis

Corresponding Author:

Prof. Kenneth N. Raymond, Department of Chemistry, University of California, Berkeley, CA 94720-  
1460 (USA). Fax: (+1) 510-486-5283. E-mail: raymond@socrates.berkeley.edu

**Abstract**

The molecular structure of the self-assembled supramolecular assembly  $[M_4L_6]^{12-}$  has been explored with different metals ( $M = Ga^{III}, Fe^{III}, Ti^{IV}$ ) and different encapsulated guests ( $NEt_4^+$ ,  $BnNMe_3^+$ ,  $Cp_2Co^+$ ,  $Cp^*_2Co^+$ ) by X-ray crystallography. While the identity of the metal ions at the vertices of the  $M_4L_6$  structure is found to have little effect on the assembly structure, encapsulated guests significantly distort the size and shape of the interior cavity of the assembly. Cations on the exterior of the assembly are found to interact with the assembly through either  $\pi$ - $\pi$ , cation- $\pi$ , or CH- $\pi$  interactions. In some cases, the exterior guests interact with only one assembly, but cations with the ability to form multiple  $\pi$ - $\pi$  interactions are able to interact with adjacent assemblies in the crystal lattice. The solvent accessible cavity of the assembly is modeled using the rolling probe method and found to range from 253 – 434  $\text{\AA}^3$ , depending on the encapsulated guest. Based on the volume of the guest and the volume of the cavity, the packing coefficient for each host-guest complex is found to range from 0.47 – 0.67.

## 1.1 Introduction

Much of the guest-binding specificity in supramolecular assemblies is derived from non-covalent interactions between the host and guest molecules; which can include coulombic, van der Waals, hydrogen-bonding, or ion-association forces, as well as steric interactions,  $\pi$ - $\pi$ , cation- $\pi$ , anion- $\pi$ , or CH- $\pi$  interactions. Such forces can be attractive or repulsive in nature and can either act either independently or cooperatively. Although most of these forces are weak, their combination upon guest inclusion in synthetic host molecules can lead to strong and specific guest binding, chiral recognition,<sup>1-5</sup> stabilization of reactive intermediates<sup>6-9</sup> and chemical catalysis.<sup>10-13</sup> These forces are not restricted to synthetic systems; they have been shown to have biological importance in enzyme active sites and the self-assembly processes of biological molecules.<sup>14-18</sup> Greater understanding of host-guest interactions may inform the design of systems with enhanced guest binding selectivities and better control over encapsulated reactivity.

The effects of host-guest intermolecular forces are often difficult to determine or deconvolute in solution, since the time-average of such interactions is generally observed. However, solid state structural analysis offers an opportunity to observe them in a static environment. Such studies have been instrumental in the identification and characterization of phenomena such as cation- $\pi$  interactions or interactions between anions and electron-deficient aromatic rings in synthetic host molecules. While molecular modeling is often used to probe the basic structural properties of self-assembled systems, direct crystallographic analysis can often provide information about the size, shape, chirality, or geometric deformations in the system which would otherwise be unobtainable.

## 1.2 Background of the $M_4L_6$ assembly

Based on rational design methods, Raymond and coworkers have explored the chemistry of synthetic supramolecular assemblies over the last decade. Assemblies of the stoichiometry  $M_4L_6$  ( $M = Ga^{III}, Al^{III}, In^{III}, Fe^{III}, Ti^{IV},$  or  $Ge^{IV}$ ,  $L = N,N'$ -bis(2,3-dihydroxybenzoyl)-1,5-diaminonaphthalene) have been developed<sup>19, 20</sup> and will be the focus of this structural study. The  $M_4L_6$  assembly is a discrete, self-assembling tetrahedron in which the four metal ions define the vertices of the structure which are bridged by the six bis-bidentate ligands. The tris-bidentate coordination of the catechol amide moieties at the metal vertices makes each vertex a stereocenter and the rigid ligands transfer the chirality of one metal vertex to the others, thereby forming the homochiral  $\Delta\Delta\Delta$  or  $\Lambda\Lambda\Lambda$  configurations.<sup>21, 22</sup> While the 12- overall charge imparts water solubility for assemblies constructed from trivalent metal vertices, the interior cavity is defined by the naphthalene walls, thereby providing a hydrophobic environment that is isolated from the bulk aqueous solution. Although initial studies of the host-guest properties mainly provided information about the scope of guest encapsulation, the chemistry of the assembly has been expanded to include mechanistic studies of guest exchange,<sup>23, 24</sup> mediation of reactivity,<sup>25, 26</sup> and use as a catalyst.<sup>10, 12, 27, 28</sup>

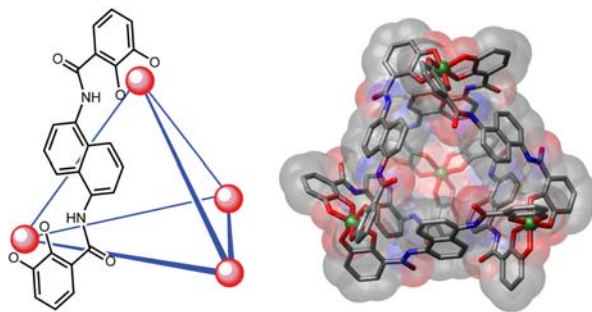


**Figure 1.** (Left) A schematic representation of the  $M_4L_6$  with only one ligand shown for clarity. (Right) A space-filling model of the assembly looking toward the aperture coincident with the 3-fold axis from which it is proposed that guests exchange.

Although the solution behavior of **1** has been studied over the last decade, questions remain about the size, shape and volume of the interior cavity of **1**, as well as how the exterior of the assembly is able to interact with guests. For example, empirical observations have shown that addition of an excess of  $\pi$ -acidic guests, such as  $Cp_2Co^+$  or  $Cp^*_2Co^+$  ( $Cp = \eta^5$ -cyclopentadienyl,  $Cp^* = \eta^5$ -pentamethylcyclopentadienyl), to an aqueous solution of **1** results in precipitation of the assembly, suggesting that these cations are able to not only bind to the interior of **1**, but also to interact strongly with its exterior. In probing the ability of cations to ion-associate to the exterior of **1**, we have previously used Pulsed Gradient Spin Echo (PGSE)  $^1H$  NMR methods to measure the diffusion coefficient of **1** in aqueous solution and have observed that hydrophobic cations, such as  $NEt_4^+$  or  $NPr_4^+$  are able to ion-associate to the exterior.<sup>29</sup> Similarly, we have obtained kinetic evidence for ion-association of hydrophobic tetraalkyl ammonium cations,<sup>24</sup> eneammonium cations,<sup>10</sup> and  $Cp^*IrL_2X^+$  complexes<sup>25</sup> during mechanistic studies of guest exchange and reaction chemistry mediated by the assembly.

From studies of guest encapsulation, we know that the assembly is able to encapsulate guests as small as  $NMe_4^+$  or as large as  $Cp^*_2Co^+$ . Based on the preference for filling empty cavities and the empirical observation by Rebek and coworkers that cavity-containing molecules tend to have 55% of their cavities filled by the encapsulated guest, we expect that the  $M_4L_6$  assembly is able to distort to

accommodate different guests.<sup>30</sup> In solution, the assembly generally exhibits *T*-symmetry (averaged on the NMR time scale), but upon encapsulation of Cp\*<sub>2</sub>Co<sup>+</sup> the symmetry of the assembly is reduced to D<sub>2</sub>.<sup>24</sup> This suggests that the guest is large enough to interact strongly with interior walls of **1** which consequently prohibits fast tumbling of the guest inside the host. This raises the question of whether the inequivalence observed by <sup>1</sup>H NMR is due to geometric or only magnetic inequivalence of the ligands.

The restricted size of the interior cavity of **1** has also been observed in reaction chemistry mediated by **1**. For the stoichiometric C-H bond activation of aldehydes by encapsulated [Cp\*(PMe<sub>3</sub>)Ir(Me)( $\eta^2$ -olefin)]<sup>+</sup>, small aldehydes are readily activated whereas larger aldehydes such as benzaldehyde are too large to enter the assembly with the iridium compound already encapsulated.<sup>25</sup> Similarly, in the rhodium-catalyzed isomerization of allylic alcohols occurring inside of the Ga<sub>4</sub>L<sub>6</sub> assembly, size selectivity is extreme with only the two smallest substrates capable of entering the assembly to undergo the reaction.<sup>26</sup> The same types of size selectivities have been observed when using the assembly as a catalyst for the hydrolysis of acid-sensitive substrates.<sup>12, 28</sup> In the hydrolysis of orthoformates, only substrates smaller than tri-*n*-pentyl orthoformate are able to enter the assembly to undergo hydrolysis. Similarly, for the hydrolysis of acetals, small acetals are readily hydrolyzed inside of the assembly whereas larger acetals are not. These data suggest an upper size limit to guests permitted entry into the interior cavity of the assembly, a limit that could be lower than the full volume of the cavity itself (*vide infra*).

In addition to the size of the assembly, the shape of the interior cavity has been important in previous host-guest chemistry. Although the chirality of the assembly is generated at each of the metal vertices, it can be transferred to the encapsulated guests and has been used for diastereoselective encapsulation of substrates such as ruthenium half-sandwich complexes<sup>31</sup> and the diastereoselective reactivity of encapsulated iridium complexes.<sup>25</sup> For both of these cases, the diastereoselectivities observed in the [Ga<sub>4</sub>L<sub>6</sub>]<sup>12-</sup> assembly are lowest for either very small or very large guests, with the optimal selectivities being obtained with guests of intermediate size. By analyzing the interior cavity

shapes and volumes, as well as the effect of charge on the cluster properties, from the molecular structure data, we hoped to learn more about the origin of this selectivity.

## 2. Results and discussion

### 2.1 Synthesis of host-guest complexes for crystallographic analysis

The host-guest complex  $(\text{NEt}_4)_7[\text{NEt}_4 \subset \text{Ti}_4\text{L}_6]$  (**3**) (where  $\subset$  denotes encapsulation) was prepared from the correct stoichiometry of  $\text{H}_4\text{L}$ ,  $\text{Ti}(\text{O}^i\text{Pr})_4$ , and  $\text{NEt}_4\text{Cl}$  in refluxing DMF as previously described.<sup>24</sup> The  $^1\text{H}$  NMR spectrum confirms formation of an octa-anionic *T*-symmetric species associated with one equivalent of encapsulated  $\text{NEt}_4^+$  and seven equivalents of exterior  $\text{NEt}_4^+$ . Crystals suitable for X-ray diffraction were grown by diffusing methanol into a DMF solution of the bulk material. The complex crystallizes in the space group  $\overline{\text{R}}\ 3\ \text{c}$  with 12 molecules in the unit cell.

The host-guest complex  $(\text{BnNMe}_3)_{11}[\text{BnNMe}_3 \subset \text{Ga}_4\text{L}_6, \text{Bn} = \text{CH}_2\text{Ph}]$  (**4**) was prepared from the  $\text{H}_4\text{L}$  ligand and  $\text{Ga}(\text{acac})_3$  using  $\text{BnNMe}_3\text{OH}$  as the base. The  $^1\text{H}$  NMR spectrum shows two different  $\text{BnNMe}_3^+$  resonances in a ratio of 11:1 corresponding to the exterior and encapsulated guest molecules. Crystals suitable for X-ray diffraction studies were obtained by diffusing acetone into a wet DMF/DMSO solution of the complex. The complex crystallizes in the space group  $P2_1/n$  with four molecules per unit cell.

The host-guest complex  $(\text{NMe}_2\text{H}_2)_{5.5}(\text{Cp}_2\text{Co})_{1.5}[\text{Cp}_2\text{Co} \subset \text{Ti}_4\text{L}_6]$  (**5**) was prepared from the  $\text{H}_4\text{L}$  ligand,  $\text{Ti}(\text{O}^i\text{Pr})_4$  and three equivalents of  $[\text{Cp}_2\text{Co}][\text{PF}_6]$  in refluxing DMF. The decomposition of DMF provided the base required to deprotonate  $\text{H}_4\text{L}$ . Crystals suitable for X-ray diffraction were obtained by diffusing methanol into a wet DMF solution of the complex. The complex crystallizes with 2.5 equivalents of  $\text{Cp}_2\text{Co}^+$  per  $\text{Ti}_4\text{L}_6$  in the space group  $\overline{\text{R}}\ 3\ \text{c}$  with twelve molecules in each unit cell.

The host-guest complex  $\text{K}_8(\text{Cp}^*\text{Co})_3[\text{Cp}^*\text{Co} \subset \text{Ga}_4\text{L}_6]$  (**6**) was prepared from the  $\text{H}_4\text{L}$  ligand,

Ga(acac)<sub>3</sub> and four equivalents of [Cp<sup>\*</sup><sub>2</sub>Co][PF<sub>6</sub>] in MeOH using KOH as the base. Crystals suitable for X-ray diffraction studies were obtained by diffusing acetone into a 5:1 solution of DMSO:MeOH. The complex crystallizes with three equivalents of Cp<sup>\*</sup><sub>2</sub>Co<sup>+</sup> per Ga<sub>4</sub>L<sub>6</sub> in the space group Fd  $\bar{3}$  c with sixteen molecules in each unit cell.

**Table 1.** Crystal data for complexes **3-6**.

	<b>3</b>	<b>4</b>	<b>5</b>	<b>6</b>
Formula	C <sub>182</sub> H <sub>111</sub> N <sub>17.5</sub> O <sub>36</sub> Ti <sub>4</sub>	C <sub>293</sub> H <sub>265</sub> Ga <sub>4</sub> N <sub>27.5</sub> O <sub>41.5</sub>	C <sub>100.75</sub> H <sub>96</sub> Co <sub>2.5</sub> N <sub>16</sub> O <sub>56.6</sub> Ti <sub>4</sub>	C <sub>204</sub> H <sub>174</sub> Co <sub>3</sub> Ga <sub>4</sub> K <sub>9</sub> N <sub>12</sub> O <sub>3</sub>
Mol. Wt.	3310.48	5144.21	3722.60	4177.12
Cryst. appearance	trigonal prism	rectangular prism	plate	cube
Cryst. color	orange	orange	red	yellow
Crystal system	trigonal	trigonal	monoclinic	cubic
Space group	R $\bar{3}$ c (#167)	P2 <sub>1</sub> /n (#14)	R $\bar{3}$ c (#167)	Fd $\bar{3}$ c (#228)
<i>a</i> [Å]	20.844(3)	26.7393(6)	20.5378(7)	50.0040(21)
<i>b</i> [Å]	20.844(3)	30.8317(2)	20.5378(7)	50.0040(21)
<i>c</i> [Å]	163.55(5)	38.5228(8)	169.966(11)	50.0040(21)
$\alpha$ [deg]	90.00	90.00	90.00	90.00
$\beta$ [deg]	90.00	109.853(1)	90.00	90.00
$\gamma$ [deg]	120.00	90.00	120.00	90.00
<i>Z</i>	12	4	12	16
<i>V</i> (Å <sup>3</sup> )	61540(25)	29871.4(9)	620867(5)	125030(9)
$\rho$ (g cm <sup>-3</sup> )	1.072	1.137	1.120	0.888
$\mu$ [mm <sup>-1</sup> ]	0.27	0.43	0.42	0.89
Cryst size [mm <sup>3</sup> ]	0.16 x 1.12 x 0.12	0.48 x 0.25 x 0.18	0.33 x 0.19 x 0.12	0.30 x 0.30 x 0.30
temp (K)	173(2)	293(2)	178(2)	173(2)
$\lambda$ (Å)	0.77490	0.71073	0.71073	0.77490
<i>F</i> (000)	20418	10686	22724	34336
$\theta$ max [deg]	19.3	19.8	17.3	22.8
Limiting indices	-17 < <i>h</i> < 17 -17 < <i>k</i> < 17 -133 < <i>l</i> < 138	-24 < <i>h</i> < 22 -16 < <i>k</i> < 29 -36 < <i>l</i> < 36	-17 < <i>h</i> < 9 -15 < <i>k</i> < 17 -141 < <i>l</i> < 141	-45 < <i>h</i> < 46 -49 < <i>k</i> < 38 -45 < <i>l</i> < 49
Meas. reflns	48435	71416	42016	73270
Independent reflns	4345	26371	4201	2738
Reflns. ( <i>I</i> > 2 $\sigma$ ( <i>I</i> ))	3636	14441	2811	1091
Parameters	426	1 634	440	177
Restraints	564	68	275	145
Data/par. ratio	10.2	16.1	9.6	15.5
R <sup>a</sup> ( <i>I</i> > 2 $\sigma$ ( <i>I</i> ))	0.154	0.128	0.157	0.146
wR <sup>b</sup> ( <i>I</i> > 2 $\sigma$ ( <i>I</i> ))	0.453	0.316	0.425	0.366
R <sup>[a]</sup> (all data)	0.170	0.205	0.192	0.224
wR <sup>[b]</sup> (all data)	0.467	0.410	0.448	0.407
GoF	2.16	1.04	1.84	1.20
$\Delta\rho_{\max}$ [e/Å <sup>3</sup> ]	+0.73	+1.16	+0.94	+0.61
$\Delta\rho_{\min}$ [e/Å <sup>3</sup> ]	-0.73	-1.61	-0.53	-0.41

[a] *R* factor definition:  $R = \sum (|F_o| - |F_c|) / \sum |F_o|$ . [b] SHELX-97 *wR* factor definition:  $wR = [\sum w(F_o^2 - F_c^2)^2 / \sum w(F_o^2)]^{1/2}$ .  
Weighting scheme:  $w = 1/[\sigma^2(F_o^2) + (np)^2]$ ,  $p = [F_o^2 + 2F_c^2]/3$ .

## 2.2 Structural Analysis

Despite the breadth of chemistry reported for  $M_4L_6$  assemblies, only two molecular structures have been reported to date due to the difficulty of growing crystals suitable for X-ray diffraction studies. The first X-ray structure of the  $M_4L_6$  assembly was that determined for the complex  $K_5(NEt_4)_6[NEt_4 \subset Fe_4L_6]$  (**1**) which crystallizes in the space group  $I\bar{4}3d$  with 16 molecules in each unit cell (CCDC-100947).<sup>19</sup> The second published structure was the enantiopure  $\Delta,\Delta,\Delta,\Delta-(NEt_4)_{11}[NEt_4 \subset Ga_4L_6]$  (**2**) which crystallizes in the space group  $I23$  with 2 molecules in the unit cell (CCDC-145431).<sup>22</sup> One challenge in crystallizing these highly-charged, highly symmetric molecules is the need to efficiently pack of unencapsulated counter ions in the crystal lattice. Depending on the charge of the metal vertices, the  $M_4L_6$  assembly either has a 12- or 8- overall charge, which, when one monocationic guest is encapsulated, leaves either 11 or 7 countercations respectively; these are difficult to efficiently pack in a high symmetry environment.

### 2.2.1 Analysis of **3**.

Comparison of the structure of  $(NEt_4)_7[NEt_4 \subset Ti_4L_6]$  (**3**) with the  $(NEt_4)_{11}[NEt_4 \subset M_4L_6]$  structures of **1** ( $M = Fe^{III}$ ) and **2** ( $M = Ga^{III}$ ) can be used to probe the effect of metal ion on the resulting assembly structure. In the structure of **3** in  $R\bar{3}c$  (Figure 2), one of the titanium atoms in the assembly and the nitrogen of the encapsulated  $NEt_4^+$  lie on the 3-fold axis (Wyckoff position  $c$ ) with the other three titanium atoms of the assembly lying on general positions. The  $Ti_4L_6$  assembly has 3-fold crystallographic symmetry, with the encapsulated guest disordered about the 3-fold axis. The crystallographic disorder of this cation was modeled with one of the methyl group carbon atoms also lying on the 3-fold axis with the adjacent methylene group disordered over three positions. Of the exterior cations, one molecule of  $NEt_4^+$  is crystallographically ordered in the asymmetric unit with pseudo  $S_4$  symmetry and is located near the catechol rings of the assembly. A second  $NEt_4^+$  cation is located near the 3-fold aperture of the assembly and is disordered. (See the supporting information for an expanded discussion of the disorder modeling).



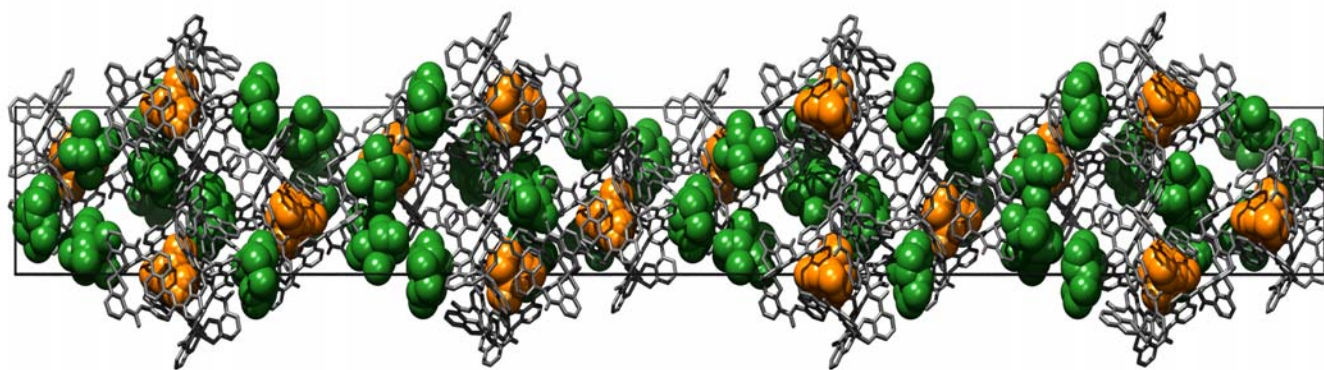


**Figure 2.** Unit cell diagram for **3** looking down the *b* axis. Hydrogen atoms and solvent have been removed for clarity. The different components of the unit cell have been color coded: host molecule (gray), encapsulated guests (orange), exterior guests (green).

(Bottom) Unit cell diagram for **5** looking down the *b* axis.

### 2.2.2 Analysis of **4**.

Crystallographic analysis of the host-guest complex containing both encapsulated and exterior  $\text{BnNMe}_3^+$  enabled investigation of how cations capable of both  $\pi$ - $\pi$  and cation- $\pi$  interactions interact with the assembly. This structure crystallizes in the lowest symmetry space group of any of the known structures of the  $\text{M}_4\text{L}_6$  assembly ( $\text{P}2_1/n$ ), with the favorable consequence that all of the  $\text{BnNMe}_3^+$  cations are crystallographically ordered (Figure 3). The cluster itself does not have crystallographic symmetry; the Ga-Ga distances range from 12.56 Å to 12.89 Å and average 12.7(1) Å.

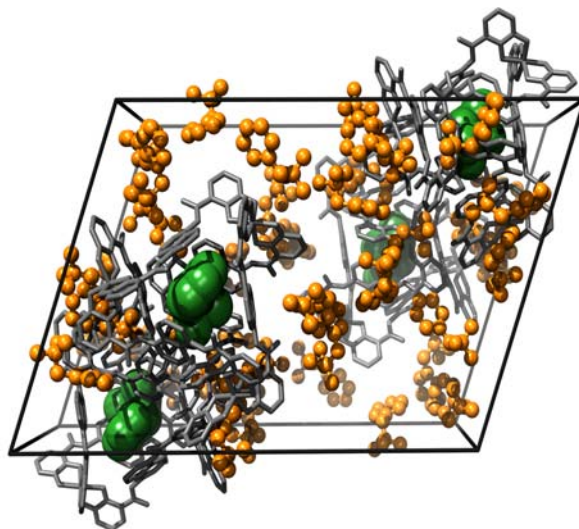


**Figure 3.** Unit cell diagram for **4**. Hydrogen atoms and solvent molecules have been removed for clarity. Different components of the unit cell have been color coded: host molecule (gray), encapsulated guests (orange), and exterior guests (green).

The encapsulated  $\text{BnNMe}_3^+$  cation interacts with the interior walls of the assembly with both  $\pi$ - $\pi$  and cation- $\pi$  interactions. The phenyl ring of the encapsulated  $\text{BnNMe}_3^+$  has a closest contact from the center of the benzene ring to a naphthalene carbon atom of 3.63 Å and an interplanar angle between the least-square plane of the phenyl ring and the naphthalene ring of 14.4°. The face of the naphthalene ring of the assembly opposite to the interacting encapsulated  $\text{BnNMe}_3^+$  does not interact with any of the cations on the exterior of the assembly. The  $\text{NMe}_3^+$  moiety of the  $\text{BnNMe}_3^+$  guest is oriented toward the three adjacent catechol rings at the vertex of the assembly with a closest contact of 3.75 Å.

The eleven remaining  $\text{BnNMe}_3^+$  cations pack around the exterior of the assembly, with some of the cations interacting with the exterior of the assembly by either  $\pi$ - $\pi$  or cation- $\pi$  interactions. All of the  $\pi$ - $\pi$  interactions to the exterior of the assembly occur between the naphthalene rings and the phenyl ring of the cation (with distances between the phenyl centroid of the  $\text{BnNMe}_3^+$  and the least-square plane of the naphthalene of 3.95 Å and 3.62 Å and interplanar angles between the least-square planes of the phenyl ring and naphthalene of 28.1° and 12.6°, respectively). The  $\text{NMe}_3^+$  moiety of the  $\text{BnNMe}_3^+$  cation interacts with the exterior of the assembly through cation- $\pi$  interactions and fits into the wedges

created by adjacent electron-rich catechol rings near the vertices of the assembly (Figure 4). None of the exterior cations bridge adjacent assemblies in the crystal.

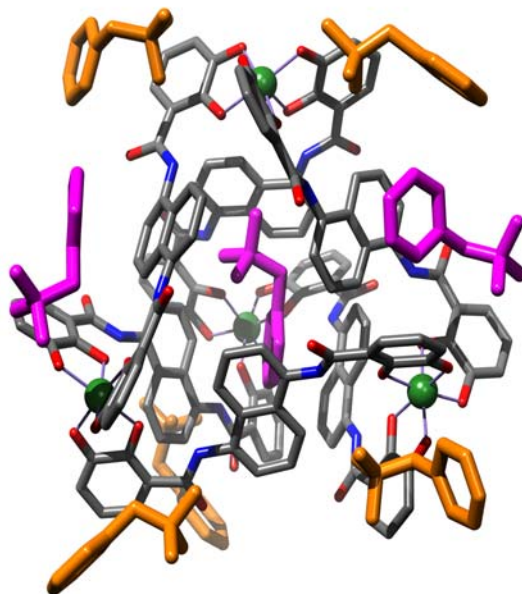


**Figure 4.** Diagram showing interactions of  $\text{NMe}_3\text{Bn}^+$  molecules with the host assembly in **4**. For clarity, different components of the assembly have been color coded: carbon (gray), nitrogen (blue), oxygen (red) and gallium (green). The  $\text{BnNMe}_3^+$  cations have been color coded based on how they interact with the assembly:  $\pi$ - $\pi$  interactions (purple), cation- $\pi$  interaction (orange).

#### 2.2.4 Analysis of **5**

The structure of  $(\text{NMe}_2\text{H}_2)_{5.5}(\text{Cp}_2\text{Co})_{1.5}[\text{Cp}_2\text{Co} \subset \text{Ti}_4\text{L}_6]$  (**5**) demonstrates that two assemblies can be bridged through  $\pi$ - $\pi$  overlap between the parallel but opposite cyclopentadienyl rings of the  $\text{Cp}_2\text{Co}^+$  and the naphthalene walls of the assembly. Similar to the structure of **3**, **5** crystallizes in  $R\bar{3}c$  (Figure 5). One of the titanium atoms from each cluster, as well as the cobalt atom of the encapsulated  $\text{Cp}_2\text{Co}^+$ , lies on the crystallographic 3-fold axis (Wyckoff position *c*) with the other titanium atoms of the host lying on general positions. The 3-fold crystallographic axis runs through the guest with a cyclopentadienyl ring centroid-Co-Ti angle of  $65^\circ$ . The atoms of the cyclopentadienyl ring were

modeled from a known structure<sup>32</sup> of  $\text{Cp}_2\text{Co}^+$  and are disordered to conform to the local site symmetry. The exterior  $\text{Cp}_2\text{Co}^+$  sits at a position with 2-fold site symmetry (Wyckoff position *e*) and is ordered in the crystal, with local  $D_{5d}$  symmetry. Due to the elongated thermal ellipsoids of carbon atoms on the cyclopentadienyl rings, the exterior  $\text{Cp}_2\text{Co}^+$  was similarly modeled to the known structure of  $\text{Cp}_2\text{Co}^+$ .

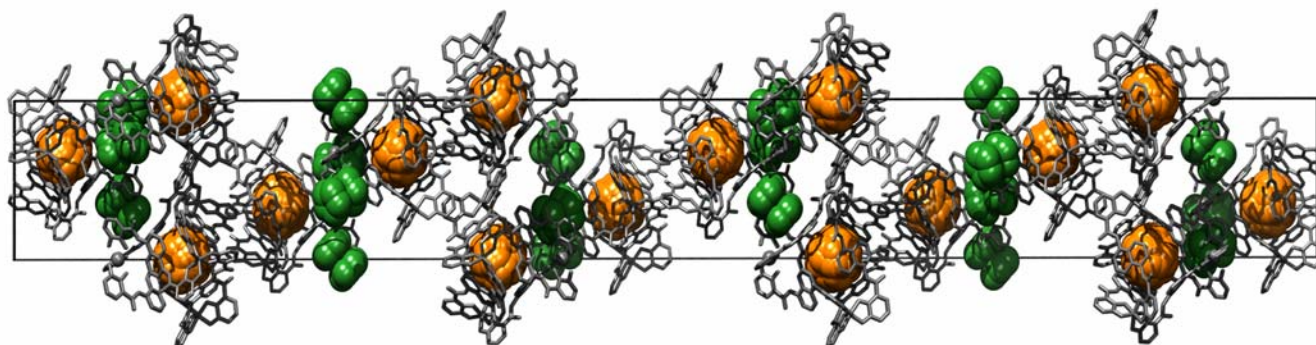


**Figure 5.** Unit cell diagram for **5** looking down the *b* axis. Hydrogen atoms, dimethylammonium counter ions, and solvent have been removed for clarity. The different components of the unit cell have been color coded: host molecule (gray), encapsulated guests (orange), exterior guests (green).

If one looks beyond the asymmetric unit of **5**, the role of the exterior 1.5  $\text{Cp}_2\text{Co}^+$  ions per tetrahedron becomes apparent. The exterior  $\text{Cp}_2\text{Co}^+$   $\pi$ -stacks between adjacent assemblies with a distance of 3.38 Å between the cyclopentadienyl ring of the  $\text{Cp}_2\text{Co}^+$  and the least-square plane of the naphthalene ring of the assembly, with an interplanar angle between the cyclopentadienyl and naphthalene rings of 4.7° (Figure 6). Each assembly in the crystal lattice interacts with three bridging  $\text{Cp}_2\text{Co}^+$  molecules, leading to the formation of groups of four  $\text{Ti}_4\text{L}_6$  assemblies and three  $\text{Cp}_2\text{Co}^+$  molecules throughout the crystal lattice (Figure 7). Also, the C-H bonds of the exterior  $\text{Cp}_2\text{Co}^+$  are in close proximity to the electron-rich catechol rings of the assembly, with a distance of 2.8 Å between the C-H bond and the least-square plane of the catechol ring (or 2.9 Å between the C-H bond and the centroid of the catechol ring) which is consistent with CH- $\pi$  interactions.

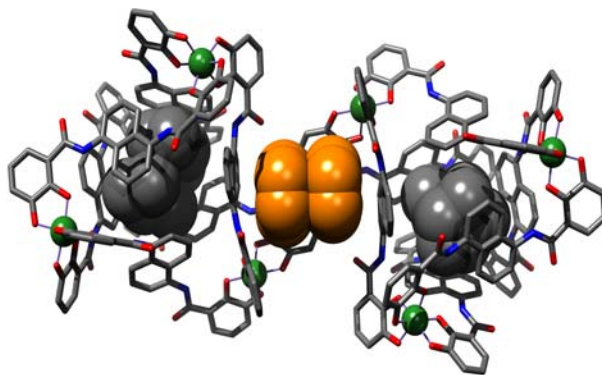


**Figure 6.** Diagram showing a  $\text{Cp}_2\text{Co}^+$  molecule bridging two host molecules by parallel but opposite  $\pi$  stacking. For clarity, different components of the unit cell have been color coded: carbon (gray), nitrogen (blue), oxygen (red), gallium (green), encapsulated guests (gray), exterior guest (orange).

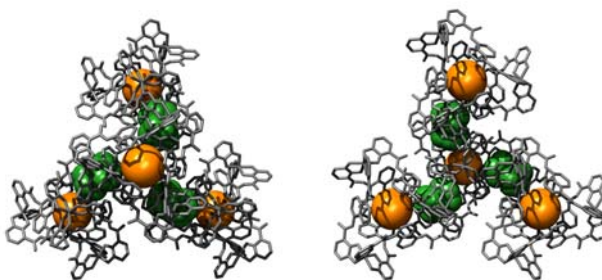


**Figure 7.** Diagram showing the interaction of the  $\text{Cp}_2\text{Co}^+$  with adjacent clusters in the unit cell. For clarity the encapsulated  $\text{Cp}_2\text{Co}^+$  is shown as a sphere (orange) and different components of the unit cell have been color coded: assembly (gray), exterior guest (green).

#### 2.2.4 Analysis of 6

Inspired by the crystallographic features of **5**, the more sterically demanding  $\text{Cp}^*_2\text{Co}^+$  was explored in  $\text{K}_9(\text{Cp}^*_2\text{Co})_2[\text{Cp}^*_2\text{Co} \subset \text{Ga}_4\text{L}_6]$  (**6**). The host-guest complex crystallizes in the space group  $\text{Fd}\bar{3}c$  such that the assembly has its full  $T$  point group symmetry (Wyckoff position  $a$ ) and the encapsulated  $\text{Cp}^*_2\text{Co}^+$  guest is disordered at the center of the assembly with this same symmetry and has an interplanar least-square plane angle of  $3.9^\circ$  relative to that of the naphthalene ring of the assembly (Figure 8). The exterior  $\text{Cp}^*_2\text{Co}^+$  lies on a special position with  $\bar{3}$  symmetry (Wyckoff position  $c$ ) Both



$\text{Cp}^*_2\text{Co}^+$  molecules were modeled from a known structure of  $\text{Cp}^*_2\text{Co}^+$  and are disordered based on the local site symmetry. Their constrained refinement with these disorder models are described in the supplementary material. The exterior  $\text{K}^+$  atoms lie on the  $d$ -glide and are disordered over three positions around the vertex of each assembly. The overall lattice has large solvent channels which lack long-range crystallographic order.

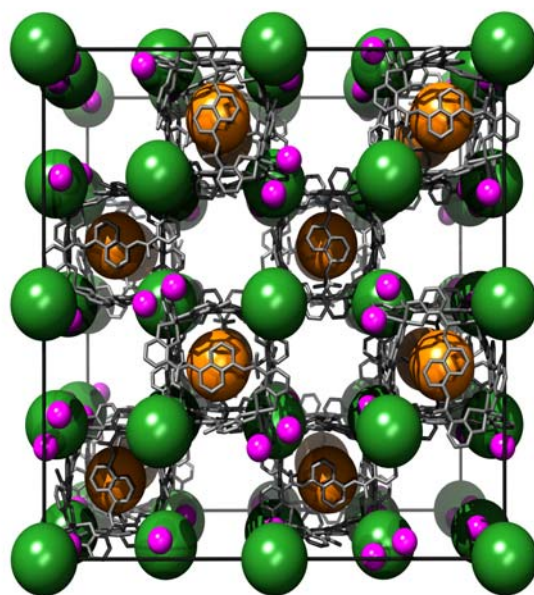


**Figure 8.** Unit cell diagram for **6**. For clarity, hydrogen atoms and solvent molecules have been removed. Disordered  $\text{Cp}^*_2\text{Co}^+$  are represented as spheres and different components of the unit cell have been color coded: host molecules (gray), potassium (purple), encapsulated guests (orange), exterior guests (green).

Stoichiometry requires two exterior  $\text{Cp}^*_2\text{Co}^+$  ions per assembly; each of these cations lies near the 3-fold aperture of the assembly (Figure 9) and they bridge adjacent assemblies throughout the lattice. The located  $\text{K}^+$  cations are near the catechol oxygen of the cluster and interact with catechol oxygens of adjacent assemblies. Based on the disorder and partial occupancy of the  $\text{K}^+$  cations, each vertex of the assembly shares one potassium atom with the adjacent assembly.

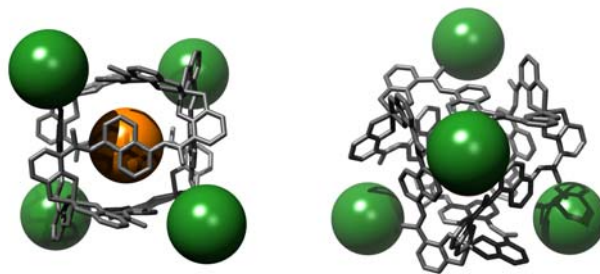


**Figure 9.** Interactions between disordered  $\text{Cp}^*_2\text{Co}^+$  cations and the host molecules. Left: Viewed down the 2-fold axis. Right: Viewed down the 3-fold axis. For clarity,  $\text{Cp}^*_2\text{Co}^+$  molecules are represented as spheres and the components have been color coded: host molecule (gray), encapsulated guest (orange), exterior guest (green).

### 2.3 Structural Comparison

The four molecular structures described above (**3-6**) as well as the two previously published crystal structures (**1-2**) were compared in order to examine how the assembly is able to accommodate differently sized guests and the structural effect of replacing the trivalent metal vertices with tetravalent  $\text{Ti}^{\text{IV}}$  ions. The assembly metrical parameters from the six  $\text{M}_4\text{L}_6$  structures are compared in Tables 2 and 3. The root mean square distances (rmsd) between each of the atoms of the assembly were calculated in order to compare the similarities between them in these structures.<sup>33</sup> As expected, the three  $\text{NET}_4^+$  structure are the most similar, with rmsd values ranging from 0.406 – 0.478 Å. In each case the differences in the twist of the naphthalene rings accounted for the majority of the distance between structures being compared.

**Table 2.** Comparison of the root mean square distances (rmsd) between structures **1-6**.<sup>34</sup>

	RMS Distance (Å)				
	2	3	4	5	6
1	0.464	0.478	0.662	0.659	0.670
2	–	0.459	0.577	0.619	0.503
3	–	–	0.609	0.646	0.576
4	–	–	–	0.571	0.544
5	–	–	–	–	0.546

In a further comparison of the six structures, the average metal-metal distances were compared; they show little deviation. In the structure of **3**, the Ti-Ti distances average 12.75 Å, similar to the 12.78 Å Fe-Fe and the 12.66 Å Ga-Ga distances in **1** and **2** respectively. The small differences are likely due to the difference in the overall charge of the assembly molecules and variations in packing of each structure.

The shortest M-M distance is 12.60 Å for **6**. This shorter M-M distance allows the naphthalene ligands to bow outward slightly to help accommodate the sterically demanding Cp\*<sub>2</sub>Co<sup>+</sup> guest. This is illustrated by comparing the average distance between opposing naphthalene centroids. The maximum of this metric is also found in structure **6**, with a naphthalene-naphthalene distance that is 0.72 Å larger than the next largest distance of 10.42 Å in the case of **3**. It might be expected that the short M-M distance of **6** would be due to greater twisting of the catecholate metal centers, and the twist angle ( $\theta$ , as defined by Kepert<sup>35, 36</sup>) for each structure was calculated for the metal vertex coincident with the crystallographic 3-fold axis. Notably, the largest twist angles (24.8° and 25.9° for structures **2** and **6** respectively) correspond to the shortest M-M distances. However, the average twist angle for the four metal centers of one structure does not correlate with M-M distance, demonstrating that these structural changes reflect the sum of many small distortions of the ligands and metal complexes of the structure.

In order to compare the maximum width of the assembly, the distance between the centroids of the opposite naphthalene walls were compared. The distance from the centroid of the naphthalene rings on opposite sides of the assembly does vary with guest. Similarly, the shape of the cavity can be greatly influenced by the angles between the mean planes of the opposing naphthalene walls. This angle varies greatly: from 47° in the case of **1** to 0° for **6**. A large naphthalene-naphthalene angle should help to transfer the chirality from the metal vertices to the interior cavity of the assembly. In addition, the distance from the center of the assembly to the centroids of the catechol rings gives a measure of how much the ligands have bowed out.



**Table 3.** Comparison of structural parameters of structures **1-6**.

	<b>1</b>	<b>2</b>	<b>3</b>	<b>4</b>	<b>5</b>	<b>6</b>
Space group	I-43d	I23	R-3c	P2 <sub>1</sub> /n	R-3c	Fd-3c
Assembly Symmetry <sup>[a]</sup>	C <sub>3</sub>	C <sub>3</sub>	C <sub>3</sub>	C <sub>1</sub>	C <sub>3</sub>	T
M-M distance (Å) <sup>[b]</sup>	12.78	12.66	12.79	12.81	12.79	12.60
Naphthalene - naphthalene (Å) <sup>[c]</sup>	10.30	10.41	10.42	10.38	10.13	11.14
Naphthalene - naphthalene (°) <sup>[d]</sup>	47.20	[g]	41.04	41.61	20.88	0.00
Center-metal (Å) <sup>[e]</sup>	7.74	8.03	7.82	7.84	7.81	7.71
Twist angle ( $\theta$ ) from C <sub>3</sub> (deg) <sup>[f]</sup>	20.2	24.8	19.8	–	16.8	25.9
<b>Average twist angle (<math>\theta_{avg}</math>) (deg)</b>	<b>18.4</b>	<b>20.2</b>	<b>21.4</b>	<b>24.2</b>	<b>20.0</b>	<b>20.4</b>

[a] Point symmetry of the assembly. [b] Taken as the average for non-cubic structures. [c] Average between the centroids of opposing naphthalene rings. [d] Average between the planes of opposing naphthalene rings. [e] Measured from the centroid of the metal vertices to each metal. [f] Measured for metal vertex with crystallographic 3-fold symmetry [g] Disorder of the naphthalene rings prohibited determination of an accurate least-square plane.

To further analyze the cavities of the host-guest complexes, the void spaces were modeled using the computer program *Voidoo*<sup>37-39</sup> which maps out the interior of the cavity using a 1.4 Å radius rolling probe. This method uses the van der Waals radii of atoms to generate a solvent-accessible surface corresponding to the cavity of the host molecule. From the analysis of the void spaces, a number of observations can be made. First, the metal vertices are inaccessible to the guest molecules, suggesting that the chirality at the metal centers cannot be directly transmitted to the encapsulated guests. This observation is also consistent with previous solution 2D <sup>1</sup>H NOESY spectroscopy, which shows strong through-space interactions between the guest and the naphthalene rather than catechol hydrogens.<sup>25, 40</sup> Secondly, the shape of the void cavity varies greatly with guest, with the shape being primarily defined by the naphthalene rings rather than the catechol moieties. The twist angle between opposing naphthalene walls has a large influence on the shape of the cavity surface. Also, the largest guest, Cp\*<sub>2</sub>Co<sup>+</sup>, greatly deforms the shape of the interior cavity, so that it resembles a cube. These observations help to explain the diastereoselectivities observed in **1**. If the guest is too small, the steric interactions with the assembly are too small to efficiently transfer the chirality of the assembly to the encapsulated guest. Conversely, if the guest is too large, distortion of the interior cavity to a pseudo-cubic void greatly diminishes the chiral induction generated by the angle between opposing naphthalene

walls of the assembly ligands. The solvent accessible shapes are shown in Figure 10 (videos of the void spaces are available in the online content associated with this article).

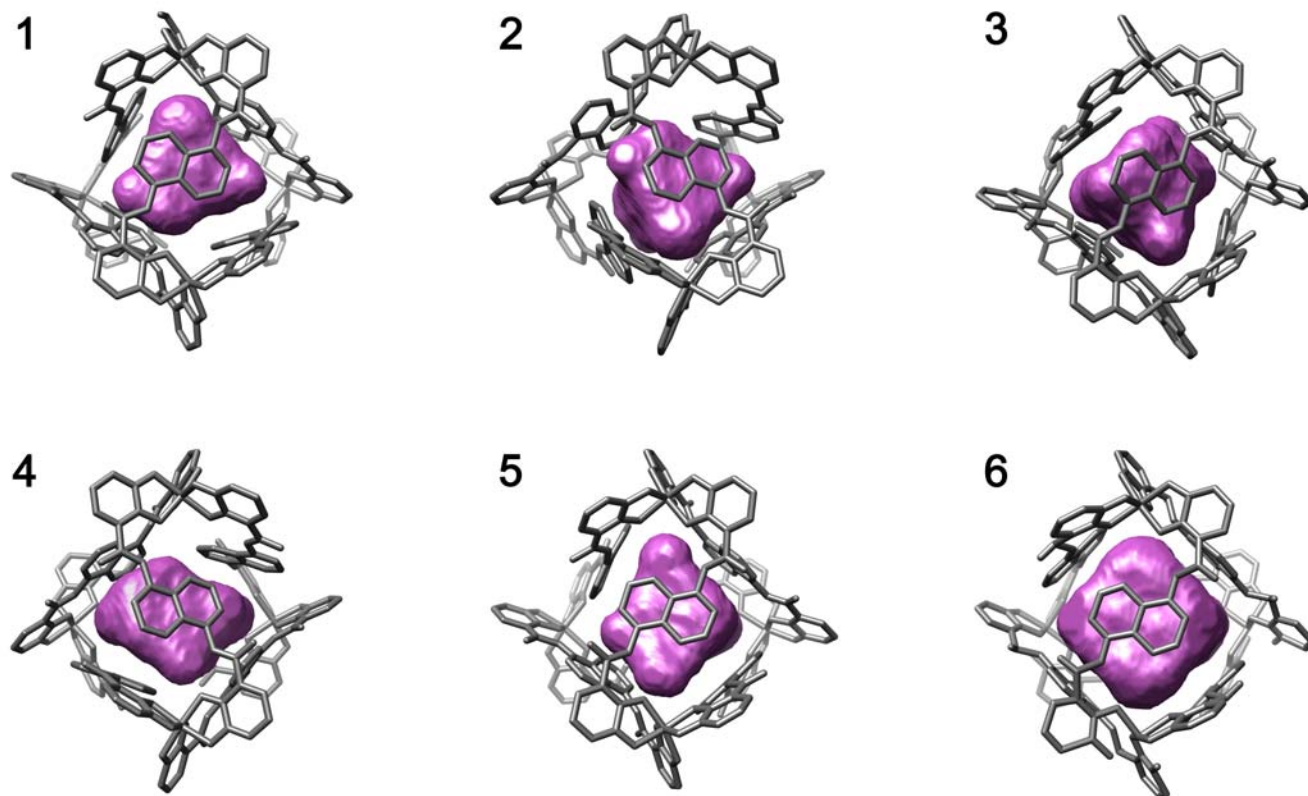


**Figure 10.** Depiction of the solvent accessible (1.4 Å rolling probe) void cavities of each of the crystal structures. Hydrogen atoms and all exterior molecules are excluded for clarity.

In order to examine how efficiently the guests pack inside the host assembly, the packing coefficients for each host-guest complex were determined. The packing coefficient is defined as the volume of the encapsulated guest (or guests) divided by the solvent accessible volume of the interior cavity, as shown in equation 1. A number of studies have investigated the packing coefficient in either calculated, synthetic, or biological host-guest structures and found that an ideal packing coefficient is  $0.55 \pm 0.09$ .<sup>30, 41-45</sup> Deviation from the 0.55 ideal generally results from other forces between either the encapsulated guest and host or between exterior molecules and the host.

$$PC = \frac{\sum_{i=1}^n v_n^i}{V_{cav}} = \frac{V_w}{V_{cav}} \quad (1)$$

**Table 4.** Cavity volumes, guest volumes, and packing coefficients for the host-guest complexes.

Structure	Volume ( $\text{\AA}^3$ )		PC
	Cavity	Guest	
<b>1</b>	261	138	0.53
<b>2</b>	253	138	0.55
<b>3</b>	293	138	0.47
<b>4</b>	285	153	0.54
<b>5</b>	270	145	0.54
<b>6</b>	434	291	0.67

The packing coefficients of the structures **1** and **2** of 0.53 and 0.55 respectively show the optimal packing of the encapsulated  $\text{NEt}_4^+$  cation (Table 4). For the other  $\text{NEt}_4^+$  containing structure, **3**, the volume of the interior cavity of the assembly is larger than in either **1** or **2**, which leads to a lower packing coefficient. It is likely that these differences arise from crystal packing forces, since compounds **1-3** all crystallize in different space groups. The structure of **4** also shows an ideal packing coefficient of 0.54. The two host guest complexes containing metallocene guests, **5** and **6**, have packing coefficients of 0.54 and 0.67 respectively. Remarkably, despite the strong  $\pi$ - $\pi$  exterior interactions in **4** and **5**, the packing coefficients remain 0.54; which is consistent with strong forces between the encapsulated guest and the host assembly in both structures. For structure **6**, containing the largest guest,  $\text{Cp}^*_2\text{Co}^+$ , the packing coefficient is significantly higher than the 0.55 ideal, suggesting that the host molecule is not able to distort enough to ideally accommodate the  $\text{Cp}^*_2\text{Co}^+$  guest. This finding supports the constrictive binding observed in solution for  $[\text{Cp}^*_2\text{Co} \subset \text{Ga}_4\text{L}_6]^{11-}$  as evidence by its slow guest exchange behavior.<sup>24</sup>

### 3. Conclusion

In summary, we have used X-ray crystallographic analysis to probe host-guest interactions between the highly-charged, self-assembled  $M_4L_6$  supramolecular cluster. Depending on the encapsulated guest, we see that intermolecular forces such as  $\pi$ - $\pi$ , cation- $\pi$ , and  $\sigma$ - $\pi$  interactions influence the binding and orientation of the encapsulated guests. Cation- $\pi$  interactions appear to be localized near the electron-rich catechol rings of the assembly and  $\pi$ - $\pi$  interactions are localized near the naphthalene walls. Changing the metal and its charge at the vertex does not have a significant effect on the geometry or shape of the host assembly. In contrast, the interior cavity of the assembly is able to distort to accommodate a wide variety of guest molecules with the shape of the internal cavity being primarily defined by the naphthalene walls of the assembly. The volume of the internal solvent-accessible cavity of the assembly ranges between 253 and 434  $\text{\AA}^3$ , depending on the encapsulated guest.

## 4. Experimental Section.

### 4.1 General

**General Procedures.** All NMR spectra were obtained using Bruker DRX-500 or AV-500 MHz spectrometers at the indicated frequencies. Chemical shifts are reported as parts per million ( $\delta$ ) and referenced to residual protic solvent peaks. The following abbreviations are used in describing NMR couplings: (s) singlet, (d) doublet, (t) triplet, (q) quartet, (b) broad, (m) multiplet. The ligand  $H_4L$ <sup>19</sup> and the host guest complex  $(NEt_4)_7[NEt_4 \subset Ti_4L_6]$ <sup>24</sup> were prepared as described in the literature. Solvents were degassed by sparging with  $N_2$  for fifteen minutes. Mass spectrometry data were acquired using a Waters QTOF API mass spectrometer equipped with a Z-spray source. Molecular graphics were constructed in ORTEP-3<sup>46</sup> and Chimera<sup>39,47</sup> and rendered in POV-Ray.

### 4.2 Synthesis of host-guest complexes

**(NBnMe<sub>3</sub>)<sub>11</sub>[NBnMe<sub>3</sub> ⊂ Ga<sub>4</sub>L<sub>6</sub>] (Structure 4).** To a degassed solution of H<sub>4</sub>L (75 mg, 0.17 mmol) in MeOH (15 mL) was added benzyltrimethylammonium hydroxide (0.34 mmol as a standardized solution ion H<sub>2</sub>O), and this yellow solution was again degassed and stirred and under N<sub>2</sub>. To this yellow solution was added Ga(acac)<sub>3</sub> (41 mg, 0.11 mmol). The solution turned deeper yellow upon addition. This solution was again degassed and stirred under nitrogen for 18 h. The volume of the solution was then concentrated to 2 mL and acetone was added (20 mL) to precipitate a fluffy, yellow solid. This was separated by centrifugation from the yellow filtrate and residual solvents were removed in vacuo: <sup>1</sup>H NMR δ 13.37 (s, 12H, NH), 8.06 (d, J = 7.6, 12H, ArH), 7.60 (d, J = 8.4, 12H, ArH), 7.46 (m, 12H + 44H, exterior BnH and cluster ArH), 6.99 (m, 12H + 11H, exterior BnH and catH), 6.20 (d, J = 6.0, 12H, catH), 6.13 (d, J = 7.6, 12H, catH), 5.39 (br t, 1H, ArH interior), 4.96 (br d, 2H, ArH interior), 4.10 (br d, 22H, exterior CH<sub>2</sub>), 3.86 (d, J = 7.6, 2H, ArH interior), 2.94 (s, 99H, exterior CH<sub>3</sub>), 0.26 (br m, 2H, interior CH<sub>2</sub>), -0.43 (s, 12H, interior CH<sub>3</sub>); ESIMS(-) (MeOH), □ = [Ga<sub>4</sub>L<sub>6</sub>]<sup>12-</sup>, ◇ = BnNMe<sub>3</sub><sup>+</sup> calcd (found), *m/z*: 1041.0 (1042.4) [□ + ◇ + 5Na<sup>+</sup> + 2H<sup>+</sup>]<sup>3-</sup>, 775.0 (776.3) [□ + ◇ + 6Na<sup>+</sup> + 2H<sup>+</sup>]<sup>4-</sup>, 615.0 (616.3) [□ + ◇ + 4Na<sup>+</sup> + 2H<sup>+</sup>]<sup>5-</sup>. X-ray quality single crystals of the dodeca(benzyltrimethylammonium) salt were obtained by slow diffusion of acetone into a wet DMF (with some DMSO to help dissolve the cluster) solution of the complex.

**(NH<sub>2</sub>Me<sub>2</sub>)<sub>5</sub>(Cp<sub>2</sub>Co)<sub>2</sub>[Cp<sub>2</sub>Co ⊂ Ti<sub>4</sub>L<sub>6</sub>] (Structure 5).** The H<sub>4</sub>L ligand (14.5 mg, 0.035 mmol), TiO(acac)<sub>2</sub> (5.56 μL, 0.021 mmol), and [CoCp<sub>2</sub>][PF<sub>6</sub>] (4.99 mg, 0.015 mmol) were combined in 600 μL of DMF-*d*<sub>7</sub>. The solution was degassed and sealed under an atmosphere of nitrogen in a J-Young NMR tube. The reaction was heated at 145-150 °C in an oil bath. At the selected time points the sample was removed and cooled to room temperature for <sup>1</sup>H NMR analysis (See Supporting Information). <sup>1</sup>H NMR (400 MHz, DMF-*d*<sub>7</sub>): δ 8.37 (d, J = 7.0 Hz, 12H, aryl); 7.93 (d, J = 8.0 Hz, 12H, aryl); 7.67 (d, J = 8.3 Hz, 12H, aryl); 7.35 (t, J = 7.7 Hz, 12H, aryl); 7.15 (d, J = 6.9 Hz, 12H, aryl); 6.47 (t, J = 6.9 Hz, 12H, aryl); 5.73 (s, 20H, Cp-H exterior), 2.21 (s, 10H, Cp-H enaps.).

**K<sub>9</sub>(Cp\*<sub>2</sub>Co)<sub>2</sub>[Cp\*<sub>2</sub>Co ⊂ Ga<sub>4</sub>L<sub>6</sub>] (Structure 6).** The H<sub>4</sub>L ligand (91.5 mg, 0.212 mmol), Ga(acac)<sub>3</sub> (52.0 mg, 0.140 mmol) and [CoCp\*<sub>2</sub>][PF<sub>6</sub>] (66.0 mg, 0.140 mmol) were suspended in methanol (50 mL) and the solution was degassed by bubbling nitrogen through it for 15 minutes. A 1.0 M methanolic solution of KOH (450 μL, 0.450 mmol) was then added, and the solution was degassed for another 15 minutes. The reaction mixture was stirred overnight at room temperature at which point some precipitate had formed. The solvent was removed under reduced pressure and the yellow residue was stirred vigorously with 15 mL of acetone, filtered, and residual solvents were removed under vacuum to yield a yellow powder. <sup>1</sup>H NMR (500 MHz, 5:1 *d*<sub>6</sub>-DMSO:*d*<sub>4</sub>-MeOH): δ 13.32 (s, 4H, NH), 12.85 (s, 4H, NH), 12.83 (s, 4H, NH), 8.28 (overlapping m, 8H, *aryl*), 7.81 (d, *J* = 7.5 Hz, 4H, *aryl*), 7.40 (d, *J* = 7.5 Hz, 4H, *aryl*), 7.30 (d, *J* = 7.5 Hz, 4H, *aryl*), 7.19 (d, *J* = 7.5 Hz, 4H, *aryl*), 7.12 (overlapping d, *J* = 8.0 Hz, 8H, *aryl*), 6.76 (d, *J* = 7.5 Hz, 4H, *aryl*), 6.66 (overlapping m, 8H, *aryl*), 6.29 (d, *J* = 7.0 Hz, 4H, *aryl*), 6.21 (overlapping m, 4H, *aryl*), 6.18 (t, *J* = 7.0 Hz, 4H, *aryl*), 1.58 (s, 90H, 3Cp\*<sub>2</sub>Co<sup>+</sup>), -0.72 (s, 30H, Cp\*<sub>2</sub>Co<sup>+</sup> encaps.). TOF MS ES(−) (MeOH / DMSO), □ = [Ga<sub>4</sub>L<sub>6</sub>]<sup>12−</sup>, ◇ = Cp\*<sub>2</sub>Co<sup>+</sup> calcd (found), *m/z*: 1449.898 (1449.902) [□ + 4◇ + 5K<sup>+</sup>]<sup>3−</sup>, 1353.152 (1353.168) [□ + 3◇ + 6K<sup>+</sup>]<sup>3−</sup>, 1256.429 (1256.433) [□ + 2◇ + 7K<sup>+</sup>]<sup>3−</sup>, 1149.703 (1159.700) [□ + ◇ + 8K<sup>+</sup>]<sup>3−</sup>, 1077.677 (1077.683) [□ + 4◇ + 4K<sup>+</sup>]<sup>4−</sup>, 1005.140 (1005.135) [□ + 3◇ + 5K<sup>+</sup>]<sup>4−</sup>, 932.576 (932.584) [□ + 2◇ + 6K<sup>+</sup>]<sup>4−</sup>, 850.531 (850.541) [□ + ◇ + 7K<sup>+</sup>]<sup>4−</sup>, 796.308 (796.315) [□ + 3◇ + 4K<sup>+</sup>]<sup>5−</sup>, 738.269 (738.277) [□ + 2◇ + 5K<sup>+</sup>]<sup>5−</sup>, 680.215 (680.236) [□ + ◇ + 6K<sup>+</sup>]<sup>5−</sup>.

### 4.3 Crystallographic Data

The diffraction data for structures **4** and **5** were collected on a Siemens SMART CCD<sup>48</sup> area detector with graphite monochromated Mo-K<sub>α</sub> radiation. The data for the structures **3** and **6** were collected at the Advanced Light Source (ALS beamline 11.3.1) (Lawrence Berkeley National Laboratory, Berkeley, USA) using monochromated synchrotron radiation ( $\lambda = 0.77490 \text{ \AA}$ ). Data were integrated by the program SAINT<sup>49</sup> and corrected for Lorentz and polarization effects. Data were analyzed for agreement and possible absorption using XPREP.<sup>50</sup> An empirical absorption correction

based on the comparison of redundant and equivalent reflections was applied using SADABS.<sup>51</sup> Equivalent reflections were merged and no decay correction was applied. Structures **3**, **5**, and **6** were solved by direct methods (SIR92)<sup>52</sup> and structure **4** was solved using Patterson methods (PATSEE)<sup>53</sup> in WinGX.<sup>54</sup> The structures were refined using Fourier techniques using SHELXL-97.<sup>55</sup> Hydrogen atoms were included but not refined. Hydrogen atoms on disordered Cp<sub>2</sub>Co<sup>+</sup>, Cp<sup>\*</sup><sub>2</sub>Co<sup>+</sup>, NEt<sub>4</sub><sup>+</sup> or solvent were not included. Hydrogen atoms were positioned geometrically, with C–H = 0.93 Å for C<sub>arom</sub>-H groups, C–H = 0.97 Å for CH<sub>2</sub> groups, and N–H = 0.89 Å and constrained to ride on their parent atoms. U<sub>iso</sub>(H) values were set at 1.2 times U<sub>eq</sub>(C) for all H atoms. For structures **3** and **6**, the electron density of the pockets of disordered solvent were calculated in Platon by the method of Spek.<sup>56</sup> In all cases, the electron density was sufficient to account for any counter ions which were not explicitly located. A discussion of the data refinement and disorder modeling for each structure is included in the Supporting Information.

**Acknowledgment.** We thank Dr. Frederick Hollander at the CHEXRAY facility for helpful discussions regarding crystallography, Dr. Ulla N. Andersen and Ákos Kókai for obtaining ESI-MS data, and Dr. Kathleen Durkin at the UCB Molecular Graphics Facility (NSF grant CHE-0233882) for assistance with volume calculations. This research and the ALS are supported by the Director, Office of Science, Office of Basic Energy Sciences (OBES), and the OBES Division of Chemical Sciences, Geosciences, and Biosciences of the U.S. Department of Energy at LBNL under Contract No. DE-AC02-05CH11231 and an NSF predoctoral fellowship to M.D.P.

**Supporting Information Available:** Crystallographic data, including crystallographic information files (CIF) and a discussion of the disorder modeling, <sup>1</sup>H NMR spectra of **3**. This material is available free of charge via the Internet at <http://pubs.acs.org>.

## References

- (1) Hembury, G. A.; Borovkov, V. V.; Inoue, Y., *Chem. Rev.* **2008**, *108*, 1-73.
- (2) Hirose, K.; Goshima, Y.; Wakebe, T.; Tobe, Y.; Naemura, K., *Anal. Chem.* **2007**, *79*, 6295 - 6302.
- (3) Aimi, J.; Oya, K.; Tsuda, A.; Aida, T., *Angew. Chem. Int. Ed.* **2007**, *46*, 2031 - 2035.
- (4) Rekharsky, M. V., et al., *J. Am. Chem. Soc.* **2006**, *128*, 14871 -14880.
- (5) Scarso, A.; Rebek, J., Jr., *Supramol. Chirality* **2006**, *265*, 1-46.
- (6) Iwasawa, T.; Hooley, R. J.; Rebek, J., Jr., *Science* **2007**, *317*, 493-496.
- (7) Dong, V. M.; Fiedler, D.; Carl, B.; Bergman, R. G.; Raymond, K. N., *J. Am. Chem. Soc.* **2006**, *128*, 14464 - 14465.
- (8) Ananchenko, G. S.; Pojarova, M.; Udachin, K. A.; Leek, D. M.; Colemanb, A. W.; Ripmeester, J. A., *Chem. Commun.* **2006**, *4*, 386-388.
- (9) Atwood, J. L.; Barbour, L. J.; Jerga, A., *J. Am. Chem. Soc.* **2002**, *124*, 2122 -2123.
- (10) Fiedler, D.; van Halbeek, H.; Bergman, R. G.; Raymond, K. N., *J. Am. Chem. Soc.* **2006**, *128*, 10240 - 10252.
- (11) Kang, J. M.; Santamaria, J.; Hilmersson, G.; Rebek, J., Jr., *J. Am. Chem. Soc.* **1998**, *120*, 7389 - 7390.
- (12) Pluth, M. D.; Bergman, R. G.; Raymond, K. N., *Science* **2007**, *316*, 85 - 88.
- (13) Yoshizawa, M.; Tamura, M.; Fujita, M., *Science* **2006**, *312*, 251 - 254.
- (14) Cerny, J.; Hobza, P., *Phys. Chem. Chem. Phys.* **2007**, *9*, 5291-5303.
- (15) Meyer, E. A.; Castellano, R. K.; Diederich, F., *Angew. Chem. Int. Ed.* **2003**, *42*, 1210-1250.
- (16) Houk, K. N.; Leach, A. G.; Kim, S. P.; Zhang, X., *Angew. Chem. Int. Ed.* **2003**, *42*, 4872 - 4897.
- (17) Paulini, R.; Muller, K.; Diederich, F., *Angew. Chem. Int. Ed.* **2005**, *44*, 1788-1805.
- (18) Mignon, P.; Loverix, S.; Steyaert, J.; Geerlings, P., **2005**, *33*, 1779-1789.
- (19) Caulder, D. L.; Powers, R. E.; Parac, T. N.; Raymond, K. N., *Angew. Chem. Int. Ed.* **1998**, *37*, 1840 - 1843.



- (20) Caulder, D. L.; Raymond, K. N., *Acc. Chem. Res.* **1999**, *32*, 975 - 982.
- (21) Davis, A. V.; Fiedler, D.; Ziegler, M.; Terpin, A.; Raymond, K. N., *J. Am. Chem. Soc.* **2007**, *129*, 15354-15363.
- (22) Terpin, A. J.; Ziegler, M.; Johnson, D. W.; Raymond, K. N., *Angew. Chem. Int. Ed.* **2001**, *40*, 157 - 160.
- (23) Davis, A. V.; Fiedler, D.; Seeber, G.; Zahl, A.; van Eldik, R.; Raymond, K. N., *J. Am. Chem. Soc.* **2006**, *128*, 1324 - 1333.
- (24) Davis, A. V.; Raymond, K. N., *J. Am. Chem. Soc.* **2005**, *127*, 7912 - 7919.
- (25) Leung, D. H.; Bergman, R. G.; Raymond, K. N., *J. Am. Chem. Soc.* **2006**, *128*, 9781 - 9797.
- (26) Leung, D. H.; Bergman, R. G.; Raymond, K. N., *J. Am. Chem. Soc.* **2007**, *129*, 2746 - 2747.
- (27) Fiedler, D.; Bergman, R. G.; Raymond, K. N., *Angew. Chem. Int. Ed.* **2004**, *43*, 6748 - 6751.
- (28) Pluth, M. D.; Bergman, R. G.; Raymond, K. N., *Angew. Chem. Int. Ed.* **2007**.
- (29) Pluth, M. D.; Tiedemann, B. E. F.; van Halbeek, H.; Nunlist, R.; Raymond, K. N., *Inorg. Chem.* **2008**, *47*, 1411-1413.
- (30) Mecozi, S.; Rebek, J., Jr., *Chem. Eur. J.* **1998**, *6*, 1016-1022.
- (31) Fiedler, D.; Leung, D. H.; Bergman, R. G.; Raymond, K. N., *J. Am. Chem. Soc.* **2004**, *126*, 3674 - 3675.
- (32) Braga, D.; Grepioni, F., *Chem. Commun.* **1998**, *8*, 911-912.
- (33) For the RMSD comparisons, the guest molecules were excluded as well as the hydrogen atoms of the assembly.
- (34) Structures were aligned along their respective crystallographic 3-fold axes. For structural comparisons with multiple rmsd settings due to symmetry, the minimum rmsd is reported in the table. The average rmsd of different settings are: 1:4 0.741, 2:4 0.691, 3:4 0.631, 4:5 0.641.
- (35) Kepert, D. L., *Inorg. Chem.* **1972**, *11*, 1561-1563.
- (36) Kepert, D. L., *Prog. Inorg. Chem.* **1977**, *23*, 1-65.
- (37) Kleywegt, G. J.; Jones, T. A., *Acta Cryst.* **1994**, *D50*, 178-185.

- (38) Kleywegt, G. J.; Zou, J. Y.; Kjeldgaard, M.; Jones, T. A., *International Tables for Crystallography, Volume F. Chapter 17.1*. 2001; Vol. pp. 353-356, 366-367.
- (39) Molecular graphics images were produced using the UCSF Chimera package from the Resource for Biocomputing, V., and Informatics at the University of California, San Francisco (supported by NIH P41 RR-01081).
- (40) Pluth, M. D.; Bergman, R. G.; Raymond, K. N., *J. Am. Chem. Soc.* **2007**, *129*, 11459 - 11467.
- (41) Zürcher, M.; Gottschalk, T.; Meyer, S.; Bur, D.; Diederich, F., *ChemMedChem* **2008**, *3*, 237 - 240.
- (42) Rekharsky, M. V., et al., *Proc. Nat. Acad. Sci. USA* **2007**, *104*, 20737-20742.
- (43) Ajami, D.; Rebek, J., Jr., *Proc. Nat. Acad. Sci. USA* **2007**, *104*, 16000-16003.
- (44) Fogarty, H. A.; Berthault, P.; Brotin, T.; Huber, G.; Desvaux, H.; Dutasta, J. P., *J. Am. Chem. Soc.* **2007**, *129*, 10332 -10333.
- (45) Watabe, T.; Kobayashi, K.; Hisaki, I.; Tohnai, N.; Miyata, M., *Bull. Chem. Soc. Jap.* **2007**, *80*, 464 - 475.
- (46) Farrugia, J. L., *J. Appl. Crystallogr.* **1997**, *30*, 565.
- (47) Pettersen, E. F.; Goddard, T. D.; Huang, C. C.; Couch, G. S.; Greenblatt, D. M.; Meng, E. C.; Ferrin, T. E., *J. Comput. Chem.* **2004**, *25*, 1605-1612.
- (48) *SMART (V5.059): Area-Detector Software Package*, Bruker Analytical X-ray Systems, Inc.: Madison, WI, (1995-99).
- (49) *SAINT (V7.07B): SAX Area-Detector Integration Program*, Siemens Industrial Automation, Inc.: Madison, WI, 2005.
- (50) *XPREP (V6.12): Part of the SHELXTL Crystal Structure Determination Package*, Bruker AXS Inc.: Madison, WI, 1995.
- (51) *SADABS (V2.10): Siemens Area Detector Absorption correction program*, George Sheldrick: 2005.

- (52) SIR92; Altomare, A.; Cascarano, G.; Giacovazzo, C.; Guagliardi, A., *J. Appl. Crystallogr.* **1993**, 26, 343-350.
- (53) Egert, E.; Sheldrick, G., *Acta Cryst.* **1985**, A41, 262-268.
- (54) Wingx 1.70.01: Farrugia, L. J., *J. Appl. Crystallogr.* **1999**, 32, 837-838.
- (55) *SHELX97 - Programs for Crystal Structure Analysis (Release 97-2)*, Sheldrick, G.M.: Institut für Anorganische Chemie der Universität, Tammanstrasse 4, D-3400 Göttingen, Germany, 1998.
- (56) Spek, A. L., *J. Appl. Cryst.* **2003**, 36, 7-13.

## Crystallographic Analysis of Guest Binding in a Highly-Charged Supramolecular Assembly: Insights into Host-Guest Interactions

Michael D. Pluth, Darren W. Johnson, Géza Szigethy, Anna V. Davis, Simon J. Teat, Allen G. Oliver, Robert G. Bergman, Kenneth N. Raymond\*

### TOC Synopsis

The molecular structure of the self-assembled supramolecular assembly  $M_4L_6$  has been characterized by X-ray crystallography. Encapsulated guests distort the size and shape of the interior cavity and unencapsulated cations interact with the exterior of the assembly through  $\pi$ - $\pi$ , cation- $\pi$ , or  $\sigma$ - $\pi$  interactions. The solvent accessible cavity of the assembly ranges from 253 – 434 Å<sup>3</sup> with associated packing coefficients of 0.47 – 0.67 depending on the encapsulated guest.

### TOC Figure

